MNRAS **000**, 1–6 (2015) Preprint 19 February 2016 Compiled using MNRAS LATEX style file v3.0

Near-IR observations of PSR J1357−6429

D. Zyuzin,[1⋆] S. Zharikov,[2] Yu. Shibanov,[1,3] A. Danilenko,[1] R. E. Mennickent[4] and A. Kirichenko[1]

[1]*Ioffe Institute, 26 Politekhnicheskaya st., St. Petersburg 194021, Russia*
[2]*Observatorio Astronómico Nacional SPM, Instituto de Astronomía, Universidad Nacional Autónoma de Mexico, Ensenada, BC, Mexico*
[3]*Peter the Great St. Petersburg Polytechnic University, 29 Politekhnicheskaya st., St. Petersburg 195251, Russia*
[4]*Department of Astronomy, Universidad de Concepcion, Casilla 160-C, Concepcion, Chile*

arXiv:1511.04233v2 [astro-ph.SR] 17 Feb 2016

Accepted XXX. Received YYY; in original form ZZZ

ABSTRACT

PSR J1357−6429 is a young radio pulsar that was detected in X-rays and γ-rays. We present the high spatial resolution near-infrared imaging of the pulsar field in J, H and K_s bands obtained with the VLT/NaCo using the Adaptive Optic system. We found a faint source at the most precise pulsar radio position which we propose as the pulsar near-infrared counterpart candidate. It is confidently detected in the J and K_s bands, with $J = 23.51\pm0.24$ and $K_s = 21.82\pm0.25$. There is a hint of the source in the H band with an upper limit $H > 22.8$. The dereddened source fluxes are compatible with the extrapolation of the pulsar X-ray spectrum towards the near-infrared. If the candidate is the true counterpart, by this property PSR J1357−6429 would be similar to the nearby middle-age pulsar PSR B0656+14. In this case, both pulsars demonstrate an unusually high near-infrared efficiency relative to the X-ray efficiency as compared to other pulsars detected in both ranges.

Key words: Pulsars: individual: PSR J1357−6429

1 INTRODUCTION

A young radio pulsar J1357−6429 (hereafter J1357) has a characteristic age $\tau = 7.3$ kyr, a period $P = 166$ ms, a spin-down luminosity $\dot{E} = 3.1 \times 10^{36}$ ergs s^{-1} and a distance of ≈ 2.5 kpc derived from the dispersion measure (Camilo et al. 2004). *XMM-Newton* and *Chandra* X-ray observations have revealed the pulsar X-ray counterpart and the pulsar wind nebula (PWN) containing a tail-like structure extended to several tens of arcseconds from the pulsar and a fainter plerion extended up to a few tens of arcminutes (Esposito et al. 2007; Zavlin 2007; Chang et al. 2012; Lemoine-Goumard et al. 2011). The plerion was detected in the TeV range with the High Energy Stereoscopic System (H.E.S.S.) and was also found in archival radio data (Abramowski et al. 2011). Based on the 7′ offset between the pulsar and the plerion centre, Abramowski et al. (2011) estimated a high pulsar transverse velocity of $650 d_{2.5} \tau_{7.3}^{-1}$ km s^{-1}, where $\tau_{7.3}$ is the pulsar age in units of 7.3 kyr and $d_{2.5}$ is the distance to the pulsar in units of 2.5 kpc. However, Abramowski et al. (2011) also noted that the plerion can be displaced by the reverse supernova remnant shock that had propagated through the non-homogeneous supernova remnant interior (Blondin et al. 2001). In that case the pulsar velocity may be much smaller.

Pulsations of J1357 with the pulsar period were discovered in X-rays with *XMM-Newton* and in the GeV range with *Fermi* (Lemoine-Goumard et al. 2011; Chang et al. 2012). The pulsar X-ray spectrum shows a thermal component originating from the surface of the neutron star (NS) and a non-thermal power-law component describing the pulsar magnetosphere emission (Lemoine-Goumard et al. 2011; Chang et al. 2012; Danilenko et al. 2012).

The J1357 field was observed in the optical *VRI* bands with the ESO Very Large Telescope (VLT) in 2009 (Mignani et al. 2011; Danilenko et al. 2012). Danilenko et al. (2012) detected a point source in all these bands within 1σ uncertainties of the pulsar X-ray position and suggested it as a pulsar optical counterpart candidate. The 5σ offset of the source from the pulsar radio interferometric position, which was obtained ≈9 years earlier (Camilo et al. 2004), implied a very high pulsar transverse velocity of $\approx 2000 d_{2.5}$ km s^{-1} (Danilenko et al. 2012). Similar velocity was obtained by Mignani et al. (2011) based on the comparison of the pulsar radio and X-ray positions. However, Kirichenko et al. (2015) showed that Camilo et al. (2004) underestimated the uncertainties of the pulsar radio position obtained with the Australia Telescope Compact Ar-

⋆ E-mail: da.zyuzin@gmail.com (DZ)

© 2015 The Authors

Table 1. Observations of PSR J1357−6429 with the VLT/NaCo under the Program 089.D-0956A.

Date	Band	Exposure × exp. number [s]	Mean airmass	Seeing range [arcsec]
2013-04-17	J	200×10	1.31	0.70–0.80
2013-03-15	H	200×10	1.32	0.83–0.89
2013-04-29	K_s	200×10	1.31	0.69–0.88

ray (ATCA) in 2000. Kirichenko et al. (2015) also presented results of the new ATCA observations performed in 2013. They found no shift of the pulsar at the 13 yr timebase between the two radio observations and put a new upper limit on the pulsar transverse velocity of $\lesssim 1200 d_{2.5}$ km yr^{-1}. Given a higher accuracy of the new ATCA pulsar position as compared to the X-ray position, they also discarded the pulsar optical counterpart proposed by Danilenko et al. (2012).

Here we report first deep near-infrared (IR) observations of the J1357 field with the VLT using the Adaptive Optics (AO) system. High spatial resolution provided by the AO system allowed us to find a new pulsar near-IR counterpart candidate which is unresolved from a bright star located within 1″ of the pulsar radio position in the previous seeing-limited VLT optical images. The observations and data reduction are described in Sect. 2, our results are presented in Sect. 3 and discussed in Sect. 4.

2 THE VLT DATA

2.1 Observations and data reduction

The pulsar field was observed in the J, H, and K_s bands with the Nasmyth Adaptive Optics System (NAOS) and Near-Infrared Imager and Spectrograph (CONICA) (in short NaCo) at the VLT/UT4 unit in the period of 2012–2013. The S27 instrument mode was used with an image scale of 0.″027/pixel and a field of view (FOV) of ∼27″×27″. A bright natural star of $V \approx$13.8 located ≈11.″2 from the target was used for AO wavefront corrections with the visual NAOS Dichroic Wavefront sensor. Several sets of 200 s dithered exposures were obtained in each band. After a preliminary inspection, we selected only sets where the observing conditions were rather stable and photometric, with seeing values varying from 0.″7 to 0.″9 (Table 1).

We performed standard near-IR data reduction, including bias subtraction, flat-fielding, sky-subtraction and cosmic-ray removal using the `IRAF` *xdimsum* package. Resulting full widths at half maximum (FWHM) of a point source near the target position on the combined J, H and K_s images were ≈ 0.″10, 0.″13 and 0.″08 at mean airmass of ≈1.3 for each band. Total integration time for each of the combined images was 2 ks.

2.2 Astrometry

As a reference frame for astrometric referencing, we used the VLT I-band image with a much wider FOV and an absolute astrometric referencing uncertainty of $\lesssim$0.″2 obtained by Danilenko et al. (2012). We selected fifteen common isolated unsaturated stars as secondary astrometric standards in this frame and in the best-quality near-IR resulting image obtained in the K_s band. Their absolute WCS coordinates were found using the optical frame. We then derived their pixel coordinates in the K_s image making use of the `IRAF` task *imcenter* with an accuracy of $\lesssim$ 0.025 of the image pixel. The `IRAF` tasks *ccmap/cctran* were applied to the astrometric transformation of the K_s image. Formal *rms* uncertainties of the astrometric fit were ΔRA $\lesssim$ 0.″05 and ΔDec. $\lesssim$ 0.″02. The resulting J and H images were aligned to the K_s frame with an accuracy of $\lesssim$ 0.″02. Combining all uncertainties and accounting for the optical astrometric referencing accuracy, a conservative estimate of our near-IR astrometric referencing uncertainty is $\lesssim$ 0.″21 for both coordinates in all three bands.

2.3 Photometric calibration

For the photometric calibration, standards 9157, 9144 and 9150 from Persson et al. (1998) were observed during the same nights as our target. We fixed the atmospheric extinction coefficients at their mean values adopted from the VLT homepage[1]: $k_J = 0.11$, $k_H = 0.06$ and $k_{K_s} = 0.07$. As a result, we obtained the following magnitude zero-points for the summed images: $J^{ZP} = 24.03 \pm 0.02$, $H^{ZP} = 23.87 \pm 0.01$ and $K_s^{ZP} = 22.99 \pm 0.01$. The 3$\sigma$ detection limits for a point-like object within several arcseconds of the target position are $J \approx 24.7$, $H \approx 23.2$ and $K_s \approx 22.7$.

3 RESULTS

3.1 Searching for a pulsar near-IR counterpart

The fragments of the resulting JHK_s images containing the pulsar are presented in Fig. 1. All sources detected and studied earlier by Danilenko et al. (2012) in the optical bands are marked following their alphabetic nomenclature, including the object C which was proposed as a possible pulsar optical counterpart. All these objects are resolved better than in the optical. The X-ray positions of the pulsar obtained from *Chandra*/HRC and *Chandra*/ACIS observations performed in 2005 and 2009, respectively, and the new pulsar radio position obtained by Kirichenko et al. (2015) are shown in the K_s image together with their 1σ error ellipses. The ellipses account for the uncertainties of the X-ray/radio position measurements and the near-IR astrometry. As seen, the most precise coordinates of the pulsar are based on the radio observations: RA = 13:57:02.525(14) and Dec. = −64:29:29.89(15)[2] (Kirichenko et al. 2015).

At this position we detected a new potential pulsar counterpart, a faint object marked by C' in Fig. 1. It also overlaps with the 1σ error ellipses of the pulsar X-ray positions. The source coordinates are RA=13:57:02.52 and Dec.=−64:29:30.15. Its 1σ uncertainty for both coordinates is 0.″22. The object is detected in the J and K_s bands at

[1] http://www.eso.org/sci/facilities/paranal/decommissioned/isaac/tools/imaging_standards.html

[2] Herein, the numbers in brackets are 1σ uncertainties referring to the last significant digits quoted.

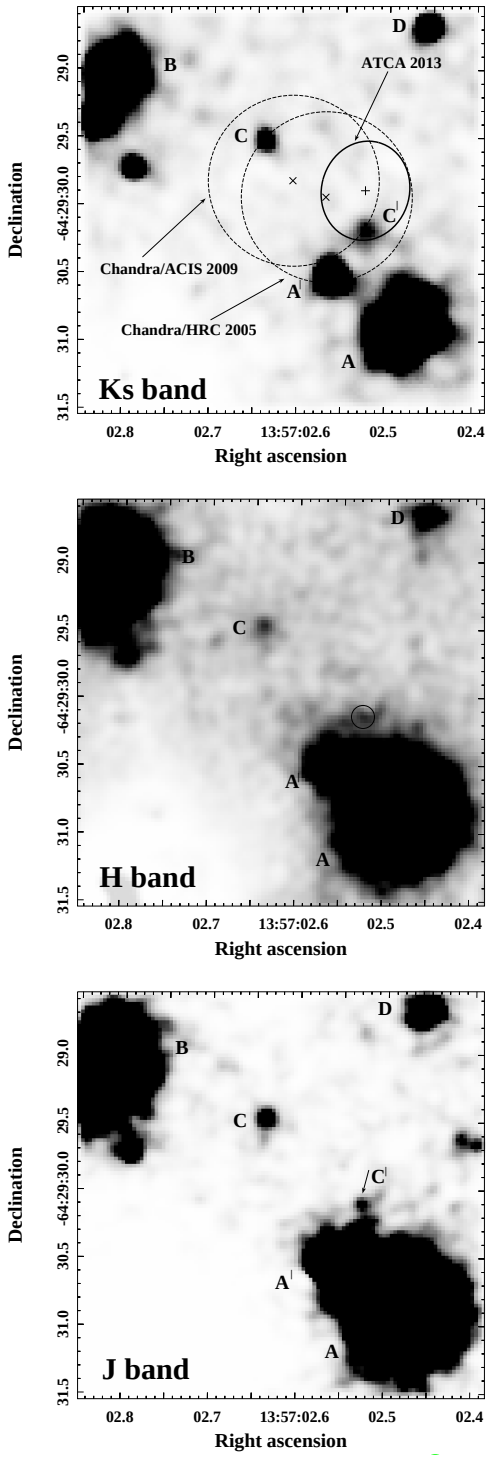

Figure 1. $3'' \times 3''$ image fragments of the J1357 field obtained with the VLT/NaCo in K_s (*top*), H (*middle*), and J (*bottom*) bands. The X-points with dashed-line circles and the + with the thick-line ellipse in the *top* panel show the pulsar positions and their 1σ uncertainties from the two *Chandra* X-ray and new ATCA radio observations, respectively. A, A', B, C, and D label objects as in Danilenko et al. (2012). C' labels the pulsar new counterpart candidate. It is not detected in the H band owing to a worse FWHM, although some flux excess is seen on its position marked by the circle.

Table 2. Measured JHK_s magnitudes of the point-like objects detected in the J1357 vicinity and labelled in Fig. 1.

Source	J	H	K_s
A	18.84(1)	18.15(1)	17.78(1)
A'	20.89(3)	20.02(4)	19.68(3)
B	19.43(1)	18.67(1)	18.32(1)
C	22.92(12)	22.06(15)	21.33(15)
C'	23.51(24)	$\gtrsim$22.8	21.82(25)
D	21.89(5)	20.88(5)	20.38(6)

$\approx 4.5\sigma$ significance. There is also a hint of the source in the H band, but a factor of 1.5 as worse FWHM in this band (Sect. 2) does not allow for a confident detection. In the VLT optical images obtained with the seeing-limited $0\farcs5$ spatial resolution, the object C' is completely hidden in the spatial profile wings of relatively bright nearby stars A and A' (see, e.g., fig. 9 from Kirichenko et al. 2015).

As in the optical (Danilenko et al. 2012), we did not find any near-IR counterpart for the extended X-ray emission of the J1357 PWN.

3.2 Photometry

We performed aperture photometry of all point-like sources labelled in Fig. 1. The respective aperture corrections were measured and applied based on the photometry of bright unsaturated field stars located near the pulsar position. We also derived a 3σ upper limit on the object C' brightness in the H band. It is not as deep as the upper limit claimed in Sect. 2.3 due to the contribution of A and A' star wings to backgrounds at the C' position. The results are collected in Table 2. The errors include the statistical measurement errors, calibration zero-points and aperture correction uncertainties. For completeness we also estimated upper limits on the object C' brightness in the VLT *VRI* images obtained by Danilenko et al. (2012): $V \gtrsim 24.6$, $R \gtrsim 24.2$ and $I \gtrsim 23.2$.

4 DISCUSSION

Considering potential optical/IR pulsar counterparts, we adopt the pulsar new radio interferometric position derived by Kirichenko et al. (2015) as the most precise one. The radio and near-IR observations were performed almost simultaneously. The only object within the 1σ error ellipse of this position is the source C' (Fig. 1). Based on the X-ray data (see Danilenko et al. 2012) a true counterpart can hardly be brighter than $K_s \approx 20.5$. In the NaCo FOV the surface number density of observed point-like objects with $K_s \gtrsim 20.5$ down to the limiting magnitude of 22.7 is $\approx$0.16 object arcsec^{-2}. The confusion probability to find an unrelated source of such brightness within the radio error ellipse with the area of ≈ 0.5 arcsec^{-2} is $\approx$0.08. Below we discuss the source C' as the counterpart candidate.

Stellar colour-magnitude and colour-colour diagrams are frequently used to distinguish pulsars from field stars by their peculiar colours (e.g., Durant et al. 2011; Mignani et al. 2011; Danilenko et al. 2012). Using the 2MASS Data Mining and the M, L and T Dwarf Archives

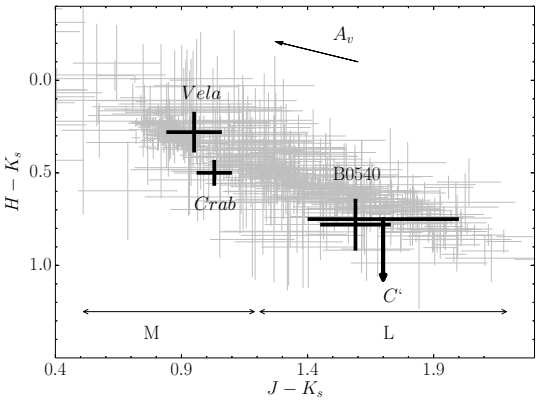

Figure 2. Colour–colour diagram of the M and L dwarfs and the observed colours of the object C'. The ranges of the L and M dwarf colours are shown by double headed arrows with respective labels. A dereddening vector marked by "Av" shows the direction and length of the shift for the object C' on the diagram for $A_V = 2$. For comparison, the colours of the Vela, Crab and B0540−69 pulsars are shown by error-bars.

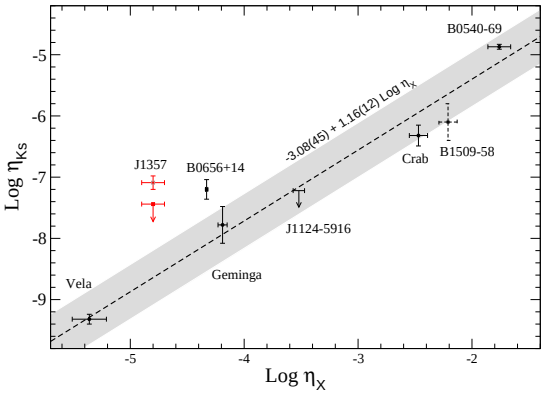

Figure 4. K_s-band efficiencies vs. X-ray efficiencies for pulsars observed in both ranges. The data are presented in Table 3. The dashed line and grey region show the best fit and its 1σ uncertainty to the data for four firmly detected near-IR pulsars (marked by black circles) excluding B0656+14. J1357 is represented by the near-IR counterpart candidate C' and by the detection limit of our observations. The near-IR counterpart candidate of PSR B1509-58 and the near-IR upper limit for PSR J1124-5916 are shown for comparison.

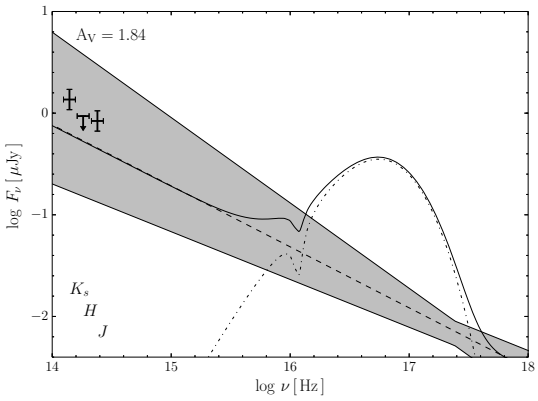

Figure 3. Tentative multi-wavelength unabsorbed spectrum of J1357. The X-ray part is described by the magnetized NS hydrogen atmosphere and power law models and is taken from Danilenko et al. (2012). The solid, dashed and dash-dotted lines are the total X-ray spectrum and contributions of the atmospheric and power law components, respectively. The grey region shows uncertainties of the power law component. The X-ray spectrum is extrapolated to the near-IR. The dereddened JK_s fluxes and the H-band upper limit for the object C' are shown by bold error bars.

from Kirkpatrick (2003), we created the near-IR colour-colour diagram shown in Fig. 2. The archival data are related to nearby dwarfs located within about 100 pc where reddening is negligible. Therefore, the star colours are consistent with their intrinsic colours. The $J-K_s$ colour of the object C' doesn't appear peculiar and would be compatible with L-type dwarf colours (Fig. 2). However, as seen from Fig. 2, the colours for other pulsars detected in the near-IR, e.g., the Crab, Vela and PSR B0540−69, are also hardly distinguishable from those of the M-L-dwarf sequence. Therefore, the near-IR colour analysis is not informative as it does not allow to confirm or disclaim the candidate as the pulsar counterpart.

Another possibility to establish the C' nature is to compare its IR fluxes with the pulsar X-ray spectral data and to see if the compiled IR-X-ray spectral energy distribution (SED) is compatible with those for other pulsars observed in both ranges. The tentative J1357 SED is presented in Fig. 3. The IR fluxes of C' are dereddened using the interstellar extinction $A_V \approx 1.84$ towards the pulsar estimated by Danilenko et al. (2012). The unabsorbed X-ray spectrum of J1357 is reproduced using the best-fit spectral parameters from the same paper. The pulsar X-ray radiation is equally well described by the magnetized NS atmosphere and blackbody spectral models for the thermal emission dominating at low energies and by the power law responsible for the high energy spectral tail. As an example, in Fig. 3 we show the result for the atmosphere model.

As seen from Fig. 3, the near-IR fluxes of the counterpart candidate are consistent within 1σ uncertainties with the long wavelength extrapolation of the pulsar X-ray spectrum. Replacing the atmosphere model with the blackbody one doesn't change this result. Similar situation is observed for the middle-aged pulsar B0656+14 (Shibanov et al. 2006; Durant et al. 2011). For other pulsars detected in the near-IR, the IR fluxes are by a factor of 10–100 lower than the X-ray extrapolation (e.g., Mignani et al. 2012; Mori et al. 2014). Therefore, if C' is the real counterpart of J1357, by its multi-wavelength spectral properties this pulsar can be similar to PSR B0656+14, which demonstrates an unusually high brightness in the near-IR.

The latter statement is also supported by the analysis of the pulsar spindown power transformation efficiencies to the X-ray and K_s-band emission. They are described by the parameters $\eta_X \equiv L_X/\dot{E}$ and $\eta_{K_s} \equiv L_{K_s}/\dot{E}$, where L_X and L_{K_s} are the X-ray nonthermal and K_s luminosities, respectively. In Table 3, we collected the related data for eight pulsars, including J1357, observed in the near-IR and X-

Table 3. Near-IR and X-ray parameters of pulsars detected in both ranges. The observed K_s magnitudes and A_V values for all pulsars except of J1357 and Vela are taken from Zharikov et al. (2013). The observed K_s magnitude for Vela is taken from Zyuzin et al. (2013). X-ray data and other parameters of pulsars are adopted from Kargaltsev & Pavlov (2008). IR data for J1357 are represented by the counterpart candidate C' and by the detection limit of our observations. The near-IR flux upper limit for PSR J1124−5916 (Zharikov et al. 2013) and the data for the near-IR counterpart candidate of PSR B1509−58 (Kaplan & Moon 2006) are included for generality.

Pulsar name	$\log\tau$	$\log\dot{E}$	distance	A_V	K_s	$\log L_{K_s}$	$\log\eta_{K_s}$	$\log L_x^{**}$	$\log\eta_x$
	yr	erg s^{-1}	kpc	mag	mag	erg s^{-1}		erg s^{-1}	
Crab	3.1	38.65	1.73(28)	1.62	13.77(5)	32.33(17)	−6.32(17)	36.19(1)	−2.47(1)
PSR 0540−69	3.2	38.17	50	0.62	18.55(10)	33.30(4)	−4.87(4)	36.41(10)	−1.76(10)
PSR B1509−58	3.2	37.25	5.2(1.4)	4.8	19.4(1)	31.18(30)	−6.1(3)	35.04(8)	−2.21(8)
PSR 1124−5916	3.5	37.08	∼ 6.0	1.98(12)	≥ 22.7	≤ 29.9	≤ −7.2	33.56(5)	−3.52(5)
PSR J1357−6429	3.8	36.49	2.5	1.84	21.82(25)	29.40(11)	−7.09(11)	31.7(1)	−4.8(1)
					≥22.7	≤29.05	≤ −7.44		
Vela	4.1	36.84	$0.293^{+0.019}_{-0.017}$	0.170(16)	21.76(6)	27.52(8)	−9.32(8)	31.48(15)	−5.36(15)
PSR B0656+14	5.0	34.58	$0.288^{+0.033}_{-0.027}$	0.09(6)	22.11(13)*	27.38(16)	−7.2(16)	30.25(1)	−4.33(1)
Geminga	5.5	34.51	$0.250^{+0.120}_{-0.060}$	0.12(9)	23.4(2)*	26.7(3)	−7.8(3)	30.32(4)	−4.19(4)

* K_s magnitude is based on the extrapolation of the SED created using the HST F110W and F160W band data.
** Logarithm of nonthermal pulsar luminosity in the 0.5–8 keV band.

rays. Only five of them have firm near-IR counterparts, while a near-IR counterpart candidate for PSR B1509−58 (Kaplan & Moon 2006) has not yet been confirmed and only an upper limit of the near-IR flux was placed for PSR J1124−5916 (Zharikov et al. 2013). In Fig. 4, we plot Log η_{K_s} vs. Log η_X. The plot demonstrates a strong correlation between these parameters. The correlation coefficient is 0.99. The positions of four firm IR pulsars in the Log η_X–Log η_{K_s} plane can be fitted by a linear regression. The best fit and its 1σ uncertainty are shown by the dashed line and the grey filled region, respectively. The regression parameters are also presented in the plot. The only pulsar, which shows a clear (about 3σ) excess of the near-IR efficiency over the fit, is PSR B0656+14. Note, that in the linear scale it overshoots the best fit by an order of magnitude. Durant et al. (2011) discussed that the excess could be due to the presence of a passive post-supernova fall-back disk around the pulsar. However, one cannot exclude that the peculiar near-IR efficiency is an intrinsic property of the PSR B0656+14 magnetosphere emission.

It is also seen from Fig. 4 that if the object C' is confirmed as the J1357 near-IR counterpart, it will be another example of a pulsar with such a peculiar near-IR efficiency. This can be important for understanding the origin of the near-IR and optical emission of pulsars. Alternatively, the position of the detection limit of our observations (Fig. 4) with respect to the best fit implies that J1357 may be about two magnitudes fainter than C'.

Unfortunately, the dereddened optical flux upper limits of the candidate obtained from the VLT data, $F_V \lesssim 2.9$ μJy, $F_R \lesssim 2.6$ μJy and $F_I \lesssim 3.8$ μJy, overshoot the X-ray extrapolation and thus are uninformative. Observations of the J1357 field in the optical using high spatial resolution imaging instruments, like the *HST*, would be useful to verify the pulsar nature of the object C' by extending its SED to shorter wavelengths. Further proper motion measurements in the radio and near-IR would be also valuable.

ACKNOWLEDGEMENTS

We thank the anonymous referee for useful comments. The work of DZ, AD and AK was supported by RFBR according to the research project No. 14-02-31600 mol_a. The work of YS was partially supported by RFBR, research projects No. 13-02-12017 ofi_m and 14-02-00868_a. SZ acknowledges support from CONACYT 151858 project. REM acknowledges support by the BASAL Centro de Astrofísica y Tecnologias Afines (CATA) PFB–06/2007. Image Reduction and Analysis Facility (`IRAF`) is distributed by the National Optical Astronomy Observatories, which are operated by the Association of Universities for Research in Astronomy, Inc., under cooperative agreement with the National Science Foundation. This research has benefited from the M, L, T and Y dwarf compendium housed at DwarfArchives.org.

REFERENCES

Abramowski A., et al., 2011, A&A, 533, A103
Blondin J. M., Chevalier R. A., Frierson D. M., 2001, ApJ, 563, 806
Camilo F., et al., 2004, ApJ, 611, L25
Chang C., Pavlov G. G., Kargaltsev O., Shibanov Y. A., 2012, ApJ, 744, 81
Danilenko A., Kirichenko A., Mennickent R. E., Pavlov G., Shibanov Y., Zharikov S., Zyuzin D., 2012, A&A, 540, A28
Durant M., Kargaltsev O., Pavlov G. G., 2011, ApJ, 743, 38
Esposito P., Tiengo A., de Luca A., Mattana F., 2007, A&A, 467, L45
Kaplan D. L., Moon D.-S., 2006, ApJ, 644, 1056
Kargaltsev O., Pavlov G. G., 2008, in Bassa C., Wang Z., Cumming A., Kaspi V. M., eds, American Institute of Physics Conference Series Vol. 983, 40 Years of Pulsars: Millisecond Pulsars, Magnetars and More. pp 171–185 (arXiv:0801.2602), doi:10.1063/1.2900138
Kirichenko A., et al., 2015, MNRAS, 452, 3273
Kirkpatrick J. D., 2003, in Martín E., ed., IAU Symposium Vol. 211, Brown Dwarfs. p. 189 (arXiv:astro-ph/0207672)
Lemoine-Goumard M., et al., 2011, A&A, 533, A102
Mignani R. P., Shearer A., de Luca A., Moran P., Collins S., Marelli M., 2011, A&A, 533, A101

Mignani R. P., De Luca A., Hummel W., Zajczyk A., Rudak B., Kanbach G., Słowikowska A., 2012, A&A, 544, A100
Mori K., et al., 2014, ApJ, 793, 88
Persson S. E., Murphy D. C., Krzeminski W., Roth M., Rieke M. J., 1998, AJ, 116, 2475
Shibanov Y. A., et al., 2006, A&A, 448, 313
Zavlin V. E., 2007, ApJ, 665, L143
Zharikov S. V., Zyuzin D. A., Shibanov Y. A., Mennickent R. E., 2013, A&A, 554, A120
Zyuzin D., Shibanov Y., Danilenko A., Mennickent R. E., Zharikov S., 2013, ApJ, 775, 101

This paper has been typeset from a TEX/LATEX file prepared by the author.